Ceria nanoparticles as promoters of CO2 electroreduction on Ni/YSZ: An efficient preparation strategy and insights into the catalytic promotion mechanism

Dingkai Chen, Mathias Barreau, Sylwia Turczyniak-Surdacka, Kamil Sobczak, Marcin Strawski, Annie Le Gal La Salle, Anna Efimenko, Detre Teschner, Corinne Petit, Spyridon Zafeiratos

Ceria nanoparticles as promoters of CO_2 electroreduction on Ni/YSZ: an efficient preparation strategy and insights into the catalytic promotion mechanism

Dingkai Chen[a], Mathias Barreau[a,], Sylwia Turczyniak-Surdacka[b,c], Kamil Sobczak[b], Marcin Strawski [b,c], Annie Le Gal La Salle,[d] Anna Efimenko,[e,f] Detre Teschner,[g,h] Corinne Petit[a] and Spyridon Zafeiratos[a,*]*

[a]Institut de Chimie et Procédés pour l'Energie, l'Environnement et la Santé, UMR 7515 du CNRS-UdS 25 Rue Becquerel, 67087 Strasbourg, France

[b]Faculty of Chemistry, Biological and Chemical Research Centre, University of Warsaw, Żwirki i Wigury 101, 02-089 Warsaw, Poland

[c]Faculty of Chemistry, University of Warsaw, Żwirki i Wigury 101, 02-089 Warsaw, Poland

[d]Institut des Matériaux Jean Rouxel (IMN), Université de Nantes-CNRS, 2 Rue de La Houssinière, BP 32229, 44322 Nantes Cedex 3, France

[e]Interface Design, Helmholtz-Zentrum Berlin für Materialien und Energie GmbH (HZB), Albert-Einstein-Str. 15, 12489 Berlin, Germany

[f]Energy Materials In-situ Laboratory Berlin (EMIL), Helmholtz-Zentrum Berlin für Materialien und Energie GmbH (HZB), Albert-Einstein-Str. 15, 12489 Berlin, Germany

[g]*Max-Planck-Institut für Chemische Energiekonversion (MPI-CEC), Stiftstrasse 34-36, D-45470 Mülheim a.d. Ruhr, Germany*

[h]*Fritz-Haber-Institut der Max-Planck-Gesellschaft, Faradayweg 4-6, D-14195 Berlin, Germany*

Supporting information 1: FTIR analysis

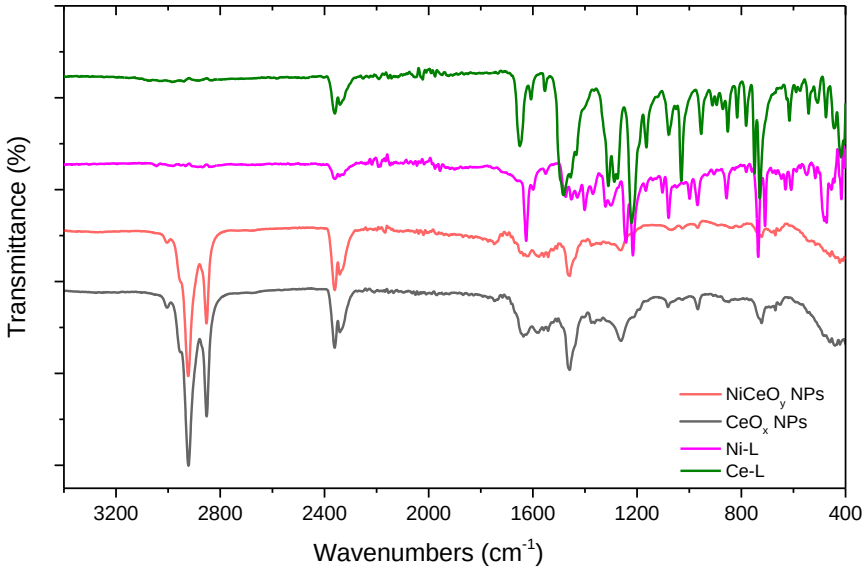

Figure S 1. FTIR spectrum of Ce (III)-L complex, Ni (II)-L complex, and as-synthesized $NiCeO_y$ and CeO_x NPs.

Supporting information 2: XRD patterns

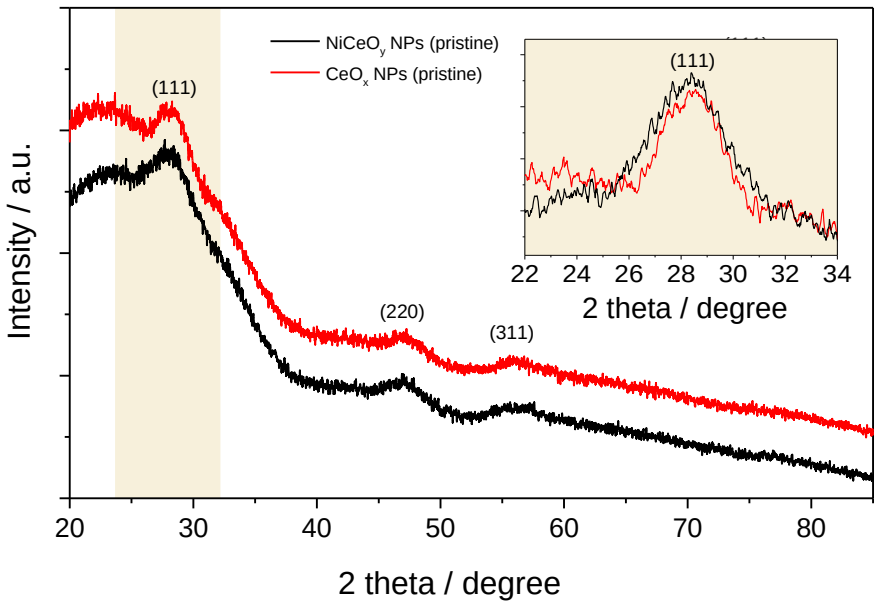

Figure S 2. XRD patterns of pristine CeO_x and $NiCeO_y$ NPs.

Supporting information 3: TEM-EDX mapping

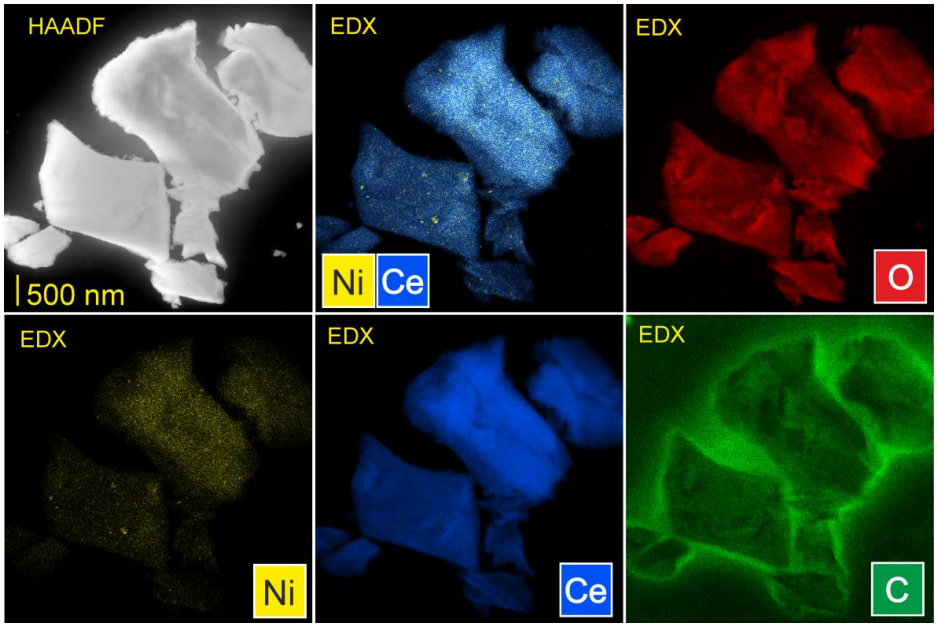

Figure S 3. HAADF-TEM and TEM-EDS elemental mapping of $NiCeO_y$ NPs samples after calcination in O_2 at 400°C.

Supporting information 4: DLS results

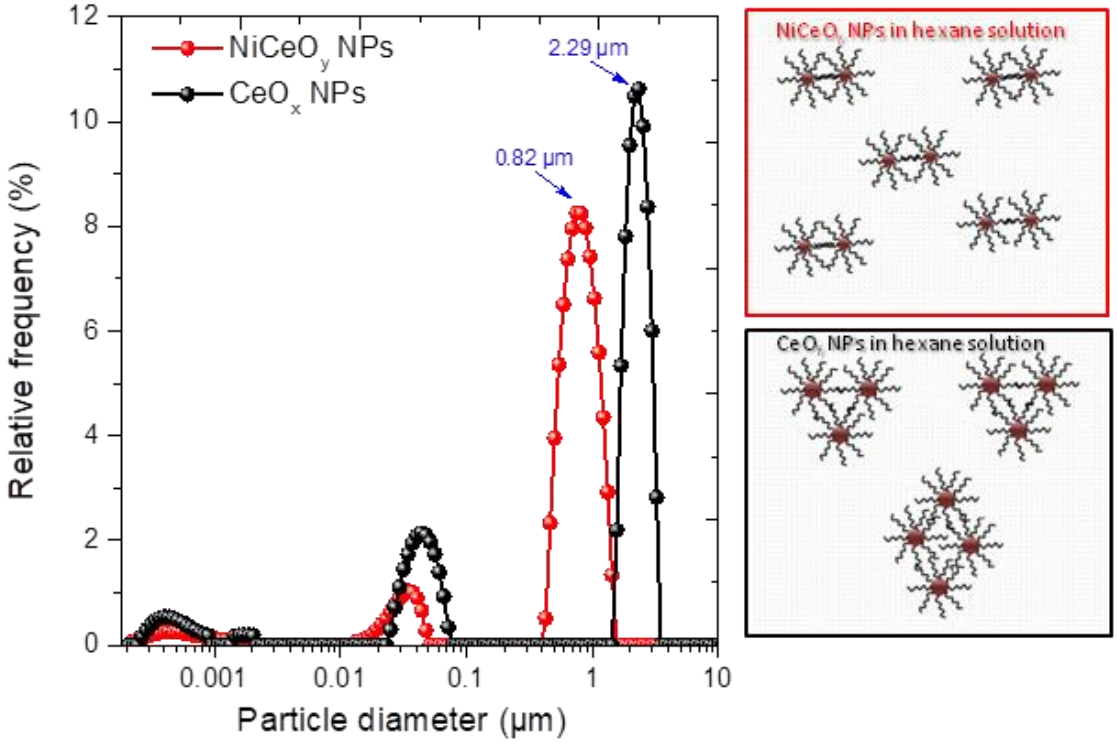

Figure S 4(a) The particle size distributions of $NiCeO_y$ and CeO_x NPs in their organic solutions in DLS measurement. (b) Schematic representation of $NiCeO_y$ and CeO_x NPs arrangement in their organic solutions.

Supporting information 5: Estimation of potential curves between $NiCeO_y$ NPs and CeO_x NPs in hexane

According to DLVO theory [1–3] the total interaction forces between two particles coated by an organic protective layer V_{Total} is the sum of van der Waals attraction V_{vdW}, and total steric repulsive forces (osmotic V_{osm} and elastic V_{elas}) [1–3].

$$V_{Total} = V_{vdW} + V_{osm} + V_{elas} \quad \text{(eq. 1)}$$

The osmotic repulsion results from the energetic balance between solvent-ligand tail and tail-tail interactions, and the elastic repulsion originates from the entropy loss that occurs upon compression of the stabilizing ligands. The dispersion stability is essentially controlled by the osmotic term since it becomes effective as soon as the ligands start to overlap, while the elastic term does not contribute significantly to V_{Total} until the ligands are forced to compress.

The V_{vdW} can be calculated based on eq. 2:

$$V_{vdW} = -\frac{A}{6}\left[\frac{2r^2}{d^2-4r^2} + \frac{2r^2}{d^2} + ln\left(\frac{d^2-4r^2}{d^2}\right)\right] \quad \text{(eq. 2)}$$

A is Hamaker constant of cerium nanoparticle in the hexane (3.5×10^{-20}J) [4], r is nanoparticles radius, d is center-to-center separation distance between two nanoparticle cores.

According to Vincent et al. [1,2,5], V_{osm} results from the energetic balance between solvent-ligand tail and tail-tail interactions, which was estimated as following:

$$V_{osm} = \frac{4\pi r k_B T}{v_{hexane}} \emptyset^2 \left(\frac{1}{2} - \chi\right)\left(l - \frac{d-2r}{2}\right)^2 \quad (l < d - 2r < 2l) \quad \text{(eq.3)}$$

$$V_{osm} = \frac{4\pi r k_B T}{v_{hexane}} \emptyset^2 \left(\frac{1}{2} - \chi\right)\left[l^2\left(\frac{d-2r}{2l} - \frac{1}{4} - ln\left(\frac{d-2r}{2}\right)\right)\right] \quad (d - 2r < l) \quad \text{(eq.4)}$$

k_B is Boltzmann's constant, v_{hexane} is the molecular volume of the solvent hexane, $\emptyset$ is the volume fraction profile of the organic species surrounded nanoparticle (oleylamine) ($\emptyset = 1 - \frac{r^3}{(r+l)^3}$), l is oleylamine length ~2 nm, and χ is the Flory-Huggins interaction parameter, which is written as the follows [3]:

$$\chi = \frac{v_{hexane}}{RT}(\delta_{hexane} - \delta_{oleylamine})^2 + 0.34 \quad \text{(eq.5)}$$

Here, R is gas constant, T is the temperature (298 K), δ_{hexane} ($14.9 MPa^{1/2}$) and $\delta_{oleylamine}$ ($16.6 MPa^{1/2}$) are the solubility parameters of hexane and oleylamine, respectively. v_{hexane} is calculated to be 2.17×10^{-28} m^3. By using eq.5 χ parameter is calculated to be 0.49.

The elastic repulsion V_{elas} originates from the entropy loss that occurs upon compression of the organic species oleylamine, namely, in the range of $d - 2r < l$.

$$V_{elas} = \frac{2\pi r k_B T l^2 \emptyset \rho_{oleylamine}}{M_{oleylamine}}\left\{x ln\left[x\left(\frac{3-x}{2}\right)^2\right] - 6ln\left(\frac{3-x}{2}\right) + 3(1-x)\right\} \quad (d - 2r < l)$$

(eq.6)

$$x = \frac{d-2r}{l} \quad \text{(eq.7)}$$

where, $\rho_{oleylamine}$ and $M_{oleylamine}$ represent the oleylamine density and molecular weight, respectively.

Table S 1. The parameters for the calculation of the potential curves of $NiCeO_y$ and CeO_x NPs in organic solution.

	$NiCeO_y$ NPs	CeO_x NPs
r (nm)[a]	1.91	2.41
l (nm)	2	2
Ø	0.88	0.84

[a]Nanoparticle radius values r are taken from XRD results of pristine cerium-based nanoparticles

Using the above values the V_{Total}, V_{vdW}, V_{osm}, and V_{elas} can be calculated based on the eq. 1-7 as shown in Figure S4. Actually, when ligands are forced to compress (the inter-particle distance $d_s < l$, with $d_s = d - 2r$)), according to the calculated result presented in the Figure S4, the repulsions including osmotic term and elastic term have small contribution, so their effect can be neglected.

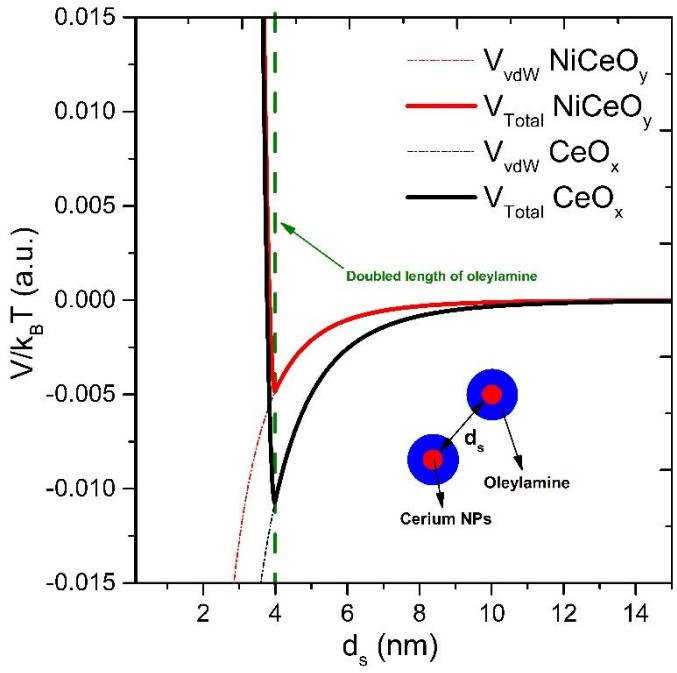

Figure S 5. The calculated total potential curves between $NiCeO_y$ and CeO_x NPs. The inter-particle distance d_s ($d_s = d - 2r$) was defined as surface-to-surface separation distance between two nanoparticles. As shown in the figure, the repulsive forces arise at the distance, where oleylamine surrounded ceria-based nanoparticles contacts each other.

Supporting information 6: Photographs during the drying treatment

Figure S6 shows photographs of two Ni/YSZ electrodes impregnated with 50 µL of $NiCeO_y$ or CeO_x solution, taken at different drying stages. In the images the organic solution appears darker than the Ni/YSZ support which has a light grey color. Just after drop-casting, the support infiltrated by the $NiCeO_y$ shows less dark areas as compared to CeO_x, indicating better spreading and pore-filling in the former case. After drying for 30 min at 80 ^{o}C, the surface of $50NiCeO_y$@Ni/YSZ seems homogenous in color, while in case of $50CeO_x$@Ni/YSZ spots with dark and light contrast remains even after 90 min at 80 ^{o}C. Since hexane evaporates fast at 80 °C (boiling point 68 °C) the homogenous surface color of $NiCeO_y$ infiltrated electrode indicates that the solution was successfully entered into the pores of the Ni/YSZ electrode. On the contrary for $50CeO_x$@Ni/YSZ the appearance of dark spots on the surface suggests that part of the solution remains on top of the electrode, allowing CeO_x NPs to form a layer on the surface of Ni/YSZ rather than penetrating into its pores.

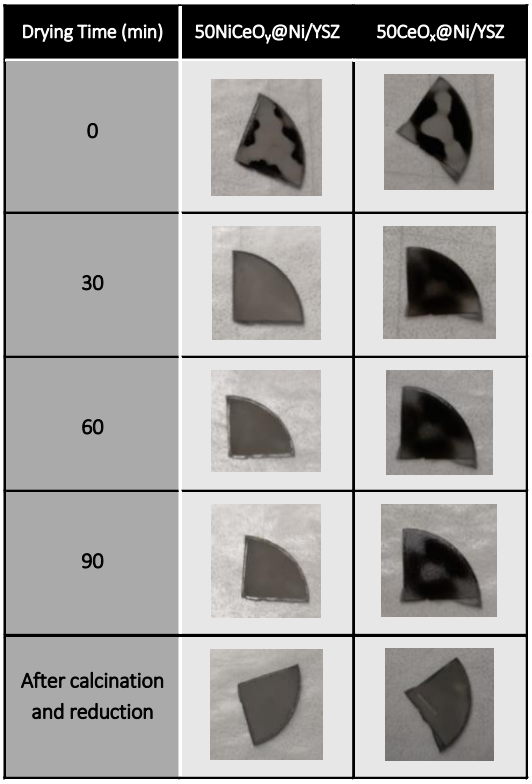

Figure S 6. Photographs of $50NiCeO_y$@Ni/YSZ and $50CeO_x$@Ni/YSZ samples during the drying treatment at 80 ^{o}C, and after calcination and reduction for 30 min in O_2 and H_2.

Supporting information 7: Laboratory XPS spectra of modified electrodes and $NiCeO_y$ NPs

The Ni 2p and Ce 3d XPS spectra of the Ni/YSZ electrode after infiltration with $NiCeO_y$ or CeO_x solutions and subsequent drying and calcination/reduction treatments (the spectra correspond to the samples at the bottom of figure S6). The spectrum of the reduced Ni/YSZ electrode before infiltration is also included for comparison. After calcination and reduction the Ni 2p signal increases for both electrodes, but in case of $50NiCeO_y$@Ni/YSZ it is notably higher (Figure S7). Since nickel signal derives principally from Ni/YSZ while Ce 3d from ceria NPs, this difference implies that less cerium remains on the surface of $50NiCeO_y$@Ni/YSZ as compared to $50CeO_2$@Ni/YSZ. Taking into account that the two impregnation solutions contain the same amount of NPs, this is indirect evidence that $NiCeO_y$ NPs are efficiently infiltrated inside the pores of Ni/YSZ.

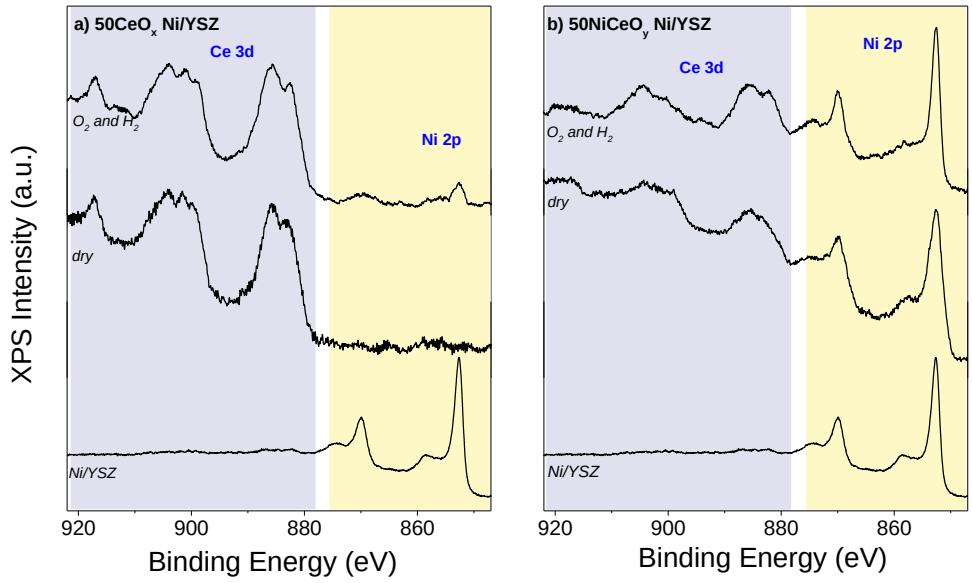

Figure S 7. The Ni 2p and Ce 3d core level XPS spectra of $50NiCeO_y$@Ni/YSZ, $50CeO_x$@Ni/YSZ as well as pristine Ni/YSZ electrode a) after drying treatment and b) after calcination and reduction treatment in O_2 at 400 °C and H_2 at 550 °C.

The spectra below show the Ni 2p and Ce 3d XPS peak of $NiCeO_y$ NPs measured by drop casting the hexane solution onto an Au foil. Evidently on the pristine sample the signal is highly attenuated due to the 2 nm oleylamine layer covering the NPs surface. After calcination the Ni 2p and Ce 3d peaks can be clearly distinguished however the intensity of Ni 2p is around 5 % of the overall. This indicates that when $NiCeO_y$ NPs precipitate on the surface of Ni/YSZ the contribution of the Ni 2p signal deriving from $NiCeO_y$ should be minor.

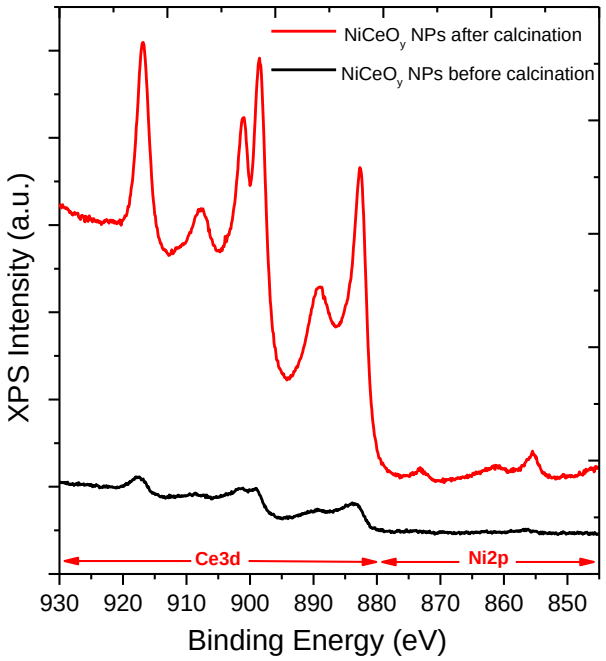

Figure S 8. Ni2p Ce3d core level XPS spectra of $NiCeO_y$ NPs before and after calcination.

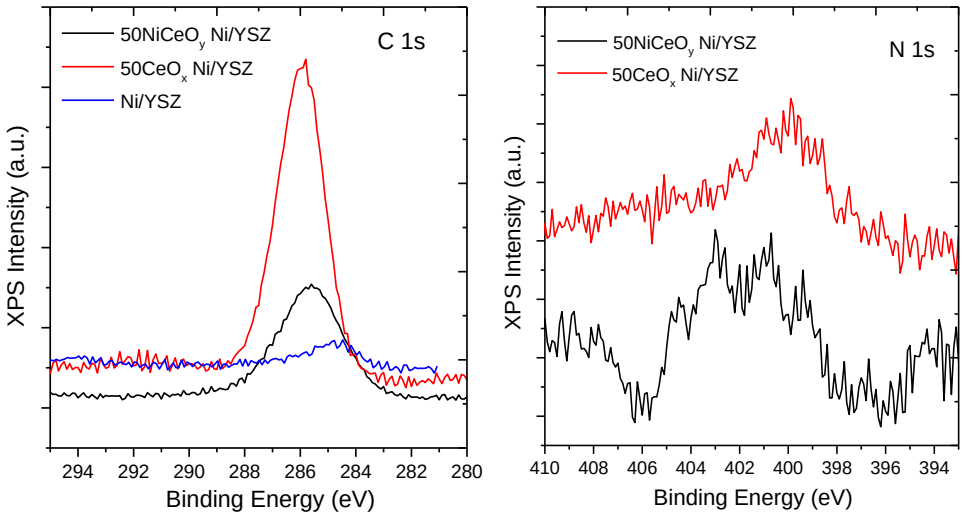

Figure S 9. C 1s and N 1s core level XPS spectra of $50NiCeO_y$@Ni/YSZ, $50CeO_x$@Ni/YSZ and Ni/YSZ after drying treatment.

Supporting information 8: *Gas phase signal during calcinations of 50NiCeO$_y$@Ni/YSZ and 50CeO$_x$@Ni/YSZ samples.*

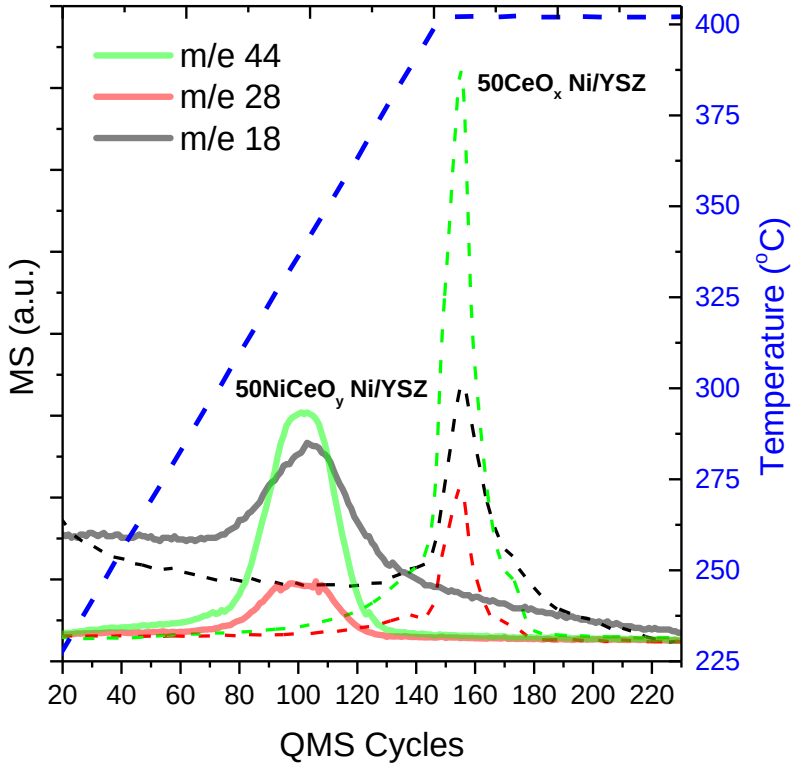

Figure S 10. Mass spectrum signal of 50NiCeO$_y$ Ni/YSZ (full lines) and 50CeO$_x$ Ni/YSZ (dashed lines) during calcination treatment in O_2.

Supporting information 9: XRD of pristine and infiltrated Ni/YSZ electrodes

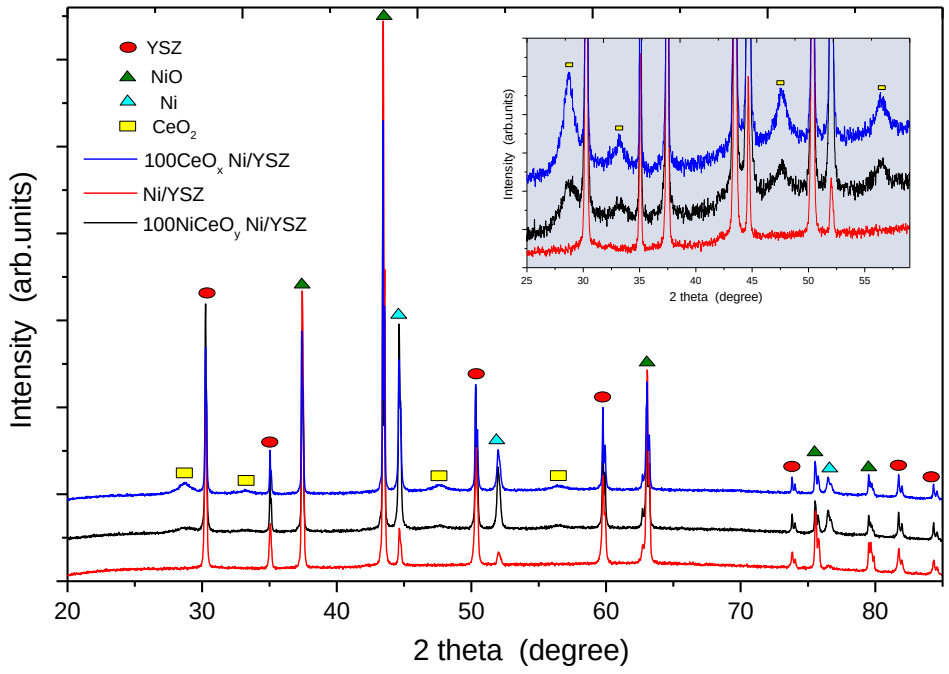

Figure S 11. XRD patterns of 100 $NiCeO_y$ Ni/YSZ, 100CeO_x Ni/YSZ as well as Ni/YSZ after two infiltration/co-firing steps (100 µl $NiCeO_y$ or CeO_x solution was dropped into Ni-YSZ through two times infiltration/co-firing steps, each time for 50µl; Prior to the each infiltration step the electrode was reduced in H_2).

Table S 2. Crystallite size results of $NiCeO_y$ and CeO_x NPs measured directly on the 100 $NiCeO_y$ Ni/YSZ and 100 CeO_x Ni/YSZ samples respectively, after two infiltration/co-firing steps.

Sample	Crystallite size (nm)
100CeO_x Ni/YSZ	9.6
100$NiCeO_y$ Ni/YSZ	6.8

Supporting information 10: Effect of the number of infiltration/co-firing steps

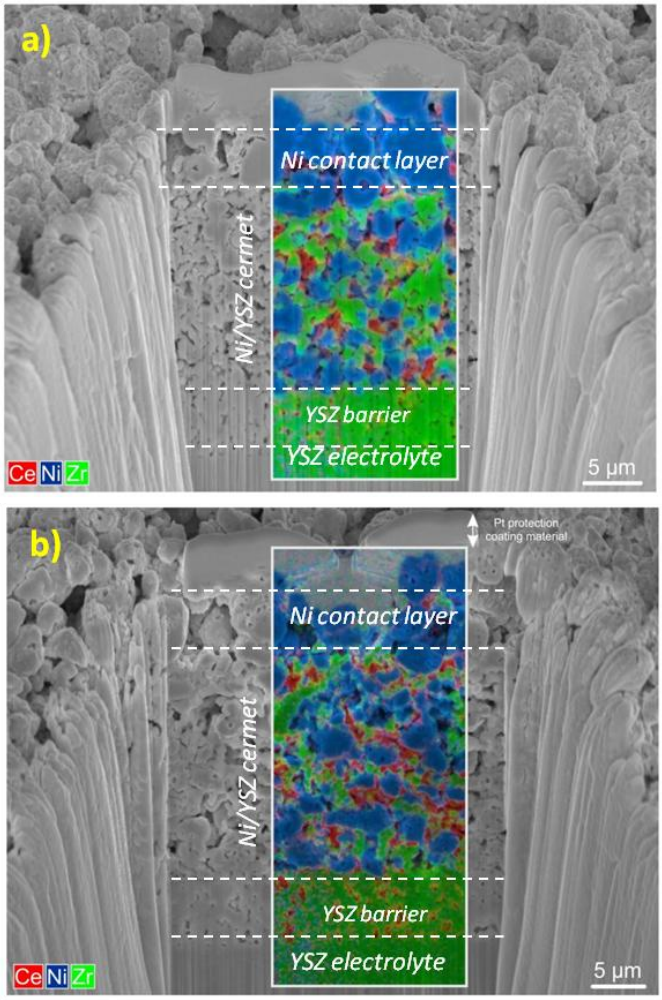

Figure S 12. Cross-sectional FIB-SEM images and the corresponding EDS elemental mapping of a) 50NiCeO$_y$@Ni/YSZ prepared in 1 infiltration/co-firing step and b) 200NiCeO$_y$@Ni/YSZ prepared in 4 infiltration/co-firing steps (4x50 µl each). After infiltration/co-firing step(s) the samples were reduced in 1 mbar H_2 at 550 °C for 30 min. The at.% of Ce as calculated from the EDS was 7.4±0.6 for 50NiCeO$_y$@Ni/YSZ and 12.4±0.6 for 200NiCeO$_y$@Ni/YSZ.

Supporting information 11: XPS survey spectra of electrodes after CO_2 electrolysis tests in the VPR reactor

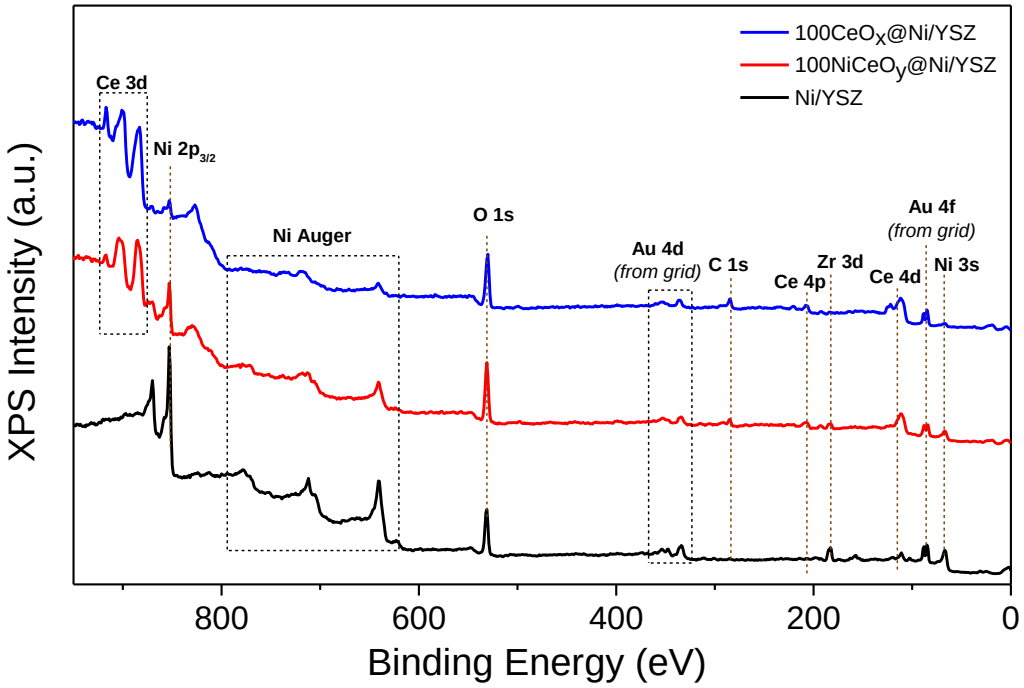

Figure S 13. XPS survey spectra of 100NiCeO$_y$@Ni/YSZ, 100CeO$_x$@Ni/YSZ and Ni/YSZ after CO_2/H_2 (96/4) electrochemical tests shown in Figure 9.

Supporting information 12: CO gas phase signal monitored by *on line* gas spectrometry analysis of the NAP-XPS chamber

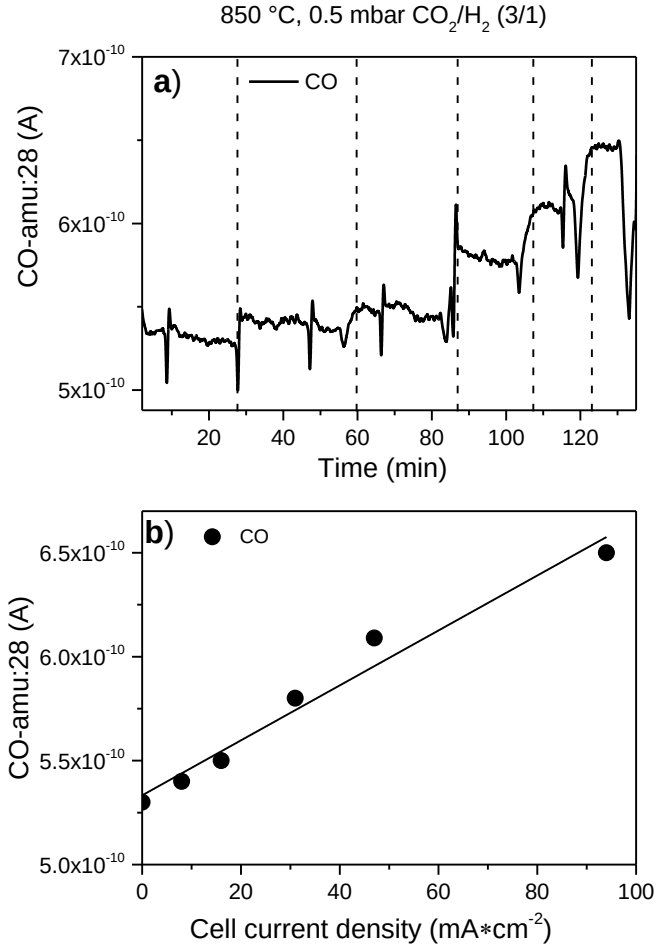

Figure S 14. The evolution CO gas phase signal as a function of **a**) time and **b**) the applied current density. The experiment was performed in the NAP-XPS chamber at 850°C in 0.5 mbar CO_2/H_2 (75/25).

Supporting information 13: NAP-XPS Ni 2p spectra of pristine Ni/YSZ electrodes under CO_2 electrolysis

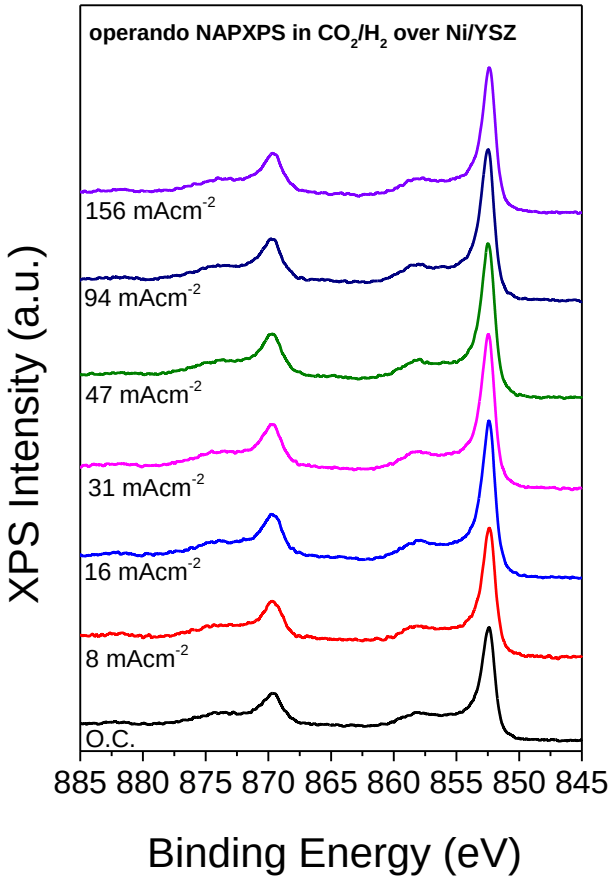

Figure S 15. NAP-XPS Ni 2p spectra of the pristine Ni/YSZ cathode recorded at 850 °C in CO_2/H_2 75/25 (0.5 mbar) under galvanostatic operation at several current densities. The spectra were recorded with hv= 1065 eV photon energy.

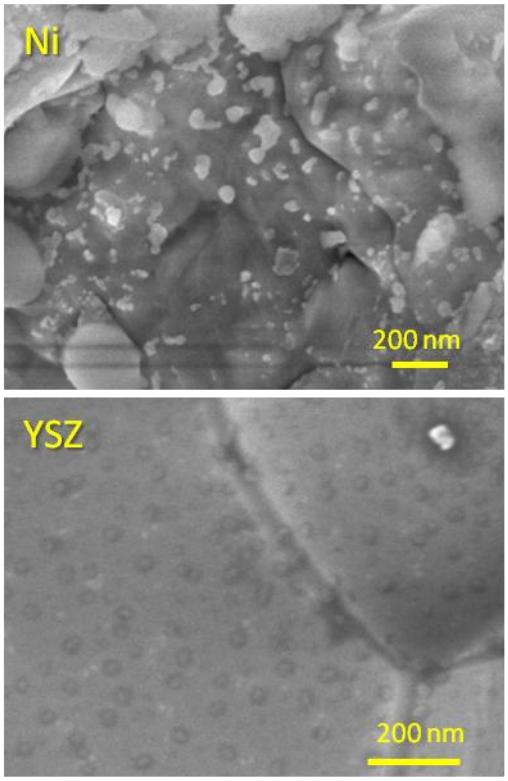

Figure S 16. SEM images of the 100NiCeO$_y$@Ni/YSZ electrodes, focusing in specific areas dominated by Ni (top) and YSZ (bottom) particles.

References

[1] P.S. Shah, J.D. Holmes, K.P. Johnston, B.A. Korgel, J. Phys. Chem. B 106 (2002) 2545–2551.

[2] T. Arita, J. Yoo, Y. Ueda, T. Adschiri, Nanoscale 2 (2010) 689–693.

[3] S. Usune, M. Ando, M. Kubo, T. Tsukada, K.I. Sugioka, O. Koike, R. Tatsumi, M. Fujita, S. Takami, T. Adschiri, J. Chem. Eng. Japan 51 (2018) 492–500.

[4] B. Faure, G. Salazar-Alvarez, A. Ahniyaz, I. Villaluenga, G. Berriozabal, Y.R. De Miguel, L. Bergström, Sci. Technol. Adv. Mater. 14 (2013).

[5] B. Vincent, J. Edwards, S. Emmett, A. Jones, Colloids and Surfaces 18 (1986) 261–281.